Optical excitations in a one-dimensional Mott insulator

Eric Jeckelmann

Fachbereich Physik, Philipps-Universität, D-35032 Marburg, Germany

(Dated: February 1, 2008)

The density-matrix renormalization-group (DMRG) method is used to investigate optical excitations in the Mott insulating phase of a one-dimensional extended Hubbard model. The linear optical conductivity is calculated using the dynamical DMRG method and the nature of the lowest optically excited states is investigated using a symmetrized DMRG approach. The numerical calculations agree perfectly with field-theoretical predictions for a small Mott gap and analytical results for a large Mott gap obtained with a strong-coupling analysis. Is is shown that four types of optical excitations exist in this Mott insulator: pairs of unbound charge excitations, excitons, excitonic strings, and charge-density-wave (CDW) droplets. Each type of excitations dominates the low-energy optical spectrum in some region of the interaction parameter space and corresponds to distinct spectral features: a continuum starting at the Mott gap (unbound charge excitations), a single peak or several isolated peaks below the Mott gap (excitons and excitonic strings, respectively), and a continuum below the Mott gap (CDW droplets).

I. INTRODUCTION

In recent years, various quasi-one-dimensional materials, such as conjugated polymers,[1,2] organic charge-transfer salts,[3,4] Cu oxides,[5] and Ni halides,[6] have been extensively studied because of their unusual optical properties and their potential application in modern optical technology. In first approximation these materials can be described as one-dimensional strongly correlated electron systems with half-filled bands. The electron-electron interaction drives such a system into a Mott insulating ground state[7,8] and dominates low-energy excitations. Therefore, the optical properties of one-dimensional Mott insulators are currently a topic of great interest.

Despite many theoretical studies, our knowledge of these systems is still fragmentary because of the difficulties associated with the investigation of strongly correlated systems. For many years, numerical exact diagonalization of small systems was the only method providing reliable information on excited states in correlated electron systems.[9,10] Recently, however, the linear optical conductivity and exciton properties of one-dimensional Mott insulators have been calculated analytically for an infinite system in the limit of a small Mott gap[11,12,13] and of a large Mott gap.[13,14,15,16,17,18] Moreover, recent developments of the density-matrix renormalization group (DMRG) method[19,20] allows one to calculate excited states and dynamical response functions numerically in large systems and with an accuracy comparable to exact diagonalizations.[11,21]

A paradigm of a one-dimensional Mott insulator is the extended Hubbard model with hopping integral t, on-site repulsion U, and nearest-neighbor repulsion V at half filling. Although this model has been widely studied, its properties are still poorly understood in the thermodynamic limit. It is known[22] that the system is a Mott insulator in a large region of the parameter space (U, V) which is physically relevant for the Coulomb repulsion between electrons ($U > V \geq 0$). The precise ground-state phase diagram has only recently be determined us-

ing DMRG.[23] In the special case of the Hubbard model[24] ($V = 0, U > 0$) the ground state is known exactly to be a Mott insulator[25] and the optical conductivity has been calculated.[11] In principle, the optical properties of the Mott insulating phase are also known for $V > 0$ at weak coupling[12,13] and at strong coupling,[13,14,15,16,17] but the range of validity of these results is not clear a priori. Results for intermediate coupling and close to the Mott phase boundary $U \approx 2V$ are scarce and the absence of finite-size-effect analysis often hinders their interpretation.[16,26,27,28]

In this paper I present an accurate and comprehensive investigation of the linear optical conductivity $\sigma_1(\omega)$ and the excited states contributing to $\sigma_1(\omega)$ in the Mott insulating phase of the one-dimensional extended Hubbard model at half filling. An efficient symmetrized DMRG[29] and the recently developed dynamical DMRG (DDMRG)[11,21] are used to calculate the optically excited states and the linear optical conductivity $\sigma_1(\omega)$ on large lattices. The comparison of numerical results for $\sigma_1(\omega)$ with field-theoretical[12,13] and strong-coupling[14] predictions confirms both the great accuracy of DDMRG and the wide validity range of both analytical methods. I have found that four types of excitations determine the optical properties in the Mott insulating phase: pairs of unbound charge excitations, excitons, excitonic strings, and charge-density-wave (CDW) droplets. I will show that each type of excitations dominate the low-energy spectrum in a particular region of the parameter space (U, V) and exhibits a distinct optical spectrum $\sigma_1(\omega)$.

The model, the linear optical conductivity $\sigma_1(\omega)$, and the relevant symmetries are introduced in detail in the next section. In Sec. III the numerical methods are briefly presented, then the estimation of DMRG truncation errors and finite-size effects are discussed. In Sec. IV I describe the four different types of excitations which contribute to the linear optical conductivity and the corresponding optical spectra in the various interaction regimes from the limit of a large Mott gap to the limit of a small Mott gap. The final section contains the

conclusion.

II. MODEL

The one-dimensional extended Hubbard model is defined by the Hamiltonian

$$
\begin{aligned}
\hat{H} \; = \; & -t \sum_{l;\sigma} \left(\hat{c}^{+}_{l,\sigma} \hat{c}_{l+1,\sigma} + \hat{c}^{+}_{l+1,\sigma} \hat{c}_{l,\sigma} \right) \\
& + U \sum_{l} \left(\hat{n}_{l,\uparrow} - \frac{1}{2} \right) \left(\hat{n}_{l,\downarrow} - \frac{1}{2} \right) \\
& + V \sum_{l} (\hat{n}_l - 1)(\hat{n}_{l+1} - 1) \; .
\end{aligned}
\tag{1}
$$

It describes electrons with spin $\sigma = \uparrow, \downarrow$ which can hop between neighboring sites. Here $\hat{c}^{+}_{l,\sigma}$, $\hat{c}_{l,\sigma}$ are creation and annihilation operators for electrons with spin σ at site l, $\hat{n}_{l,\sigma} = \hat{c}^{+}_{l,\sigma} \hat{c}_{l,\sigma}$ are the corresponding density operators, and $\hat{n}_l = \hat{n}_{l,\uparrow} + \hat{n}_{l,\downarrow}$. The hopping integral $t > 0$ gives rise to a a single-electron band of width $4t$. The Coulomb repulsion is mimicked by a local Hubbard interaction U, and a nearest-neighbor interaction V. The physically relevant parameter regime is $U > V \geq 0$. The number of electrons equals the number of lattice sites N (half-filled band). This system is in a Mott insulating phase for $V < V_c(U) \approx U/2$ (Ref.22). Precise values of the Mott phase boundary $V_c(U)$ are given in Ref. 23.

Note that the chemical potential is chosen in such a way that the Hamiltonian (1) explicitly exhibits a particle-hole symmetry. This Hamiltonian has two other discrete symmetries which are useful for optical excitation calculations: a spin-flip symmetry and a spatial reflection symmetry (through the lattice center). Therefore, each eigenstate has a well-defined parity under charge conjugation ($P_c = \pm 1$) and spin flip ($P_s = \pm 1$), and belongs to one of the two irreducible representations, A_g or B_u, of a one-dimensional lattice reflection symmetry group.

Spectroscopy with electromagnetic radiation is a common experimental probe of solid-state materials.[30] The linear (one-photon) optical absorption is proportional to the real part $\sigma_1(\omega)$ of the optical conductivity. For $\omega \neq 0$, $\sigma_1(\omega)$ is related to the imaginary part of the current-current correlation function by

$$
\sigma_1(\omega) = \frac{\text{Im}\{\chi(\omega)\}}{\omega} \; .
\tag{2}
$$

For $\omega \geq 0$ the current-current correlation function is given by

$$
\begin{aligned}
\chi(\omega > 0) \; &= \; -\frac{1}{Na} \left\langle 0 \left| \hat{J} \frac{1}{E_0 - \hat{H} + \hbar\omega + i\eta} \hat{J} \right| 0 \right\rangle \\
&= \; -\frac{1}{Na} \sum_n \frac{|\langle 0 | \hat{J} | n \rangle|^2}{\hbar\omega - (E_n - E_0) + i\eta} \; ,
\end{aligned}
\tag{3}
$$

where a is the lattice spacing. Here, $|0\rangle$ is the ground state of the Hamiltonian $\hat{H}$, $|n\rangle$ are excited states of $\hat{H}$, and E_0, E_n are their respective eigenenergies. Although $\eta = 0^+$ is infinitesimal, a finite value may be used to broaden the resonances at $\hbar\omega = E_n - E_0$ and to reduce finite-size effects. $\hat{J}$ is the current operator

$$
\hat{J} = \frac{iaet}{\hbar} \sum_{l;\sigma} \left(\hat{c}^{+}_{l,\sigma} \hat{c}_{l+1,\sigma} - \hat{c}^{+}_{l+1,\sigma} \hat{c}_{l,\sigma} \right) \; ,
\tag{4}
$$

where $-e$ is the charge of an electron. I set $a = e = \hbar = 1$ throughout, and $t = 1$ is used in figures showing the optical conductivity, which means that $\sigma_1(\omega)$ is given in units of $e^2 a/\hbar$ and ω in units of $t/\hbar$.

We note that the current operator is invariant under the spin-flip transformation but antisymmetric under charge conjugation and spatial reflection. Therefore, if the ground state $|0\rangle$ belongs to the symmetry subspace $A_g^+ \equiv (A_g, P_c, P_s)$, only excited states $|n\rangle$ belonging to the symmetry subspace $B_u^- \equiv (B_u, -P_c, P_s)$ contribute to the optical conductivity. According to selection rules, the matrix element $\langle 0 | \hat{J} | n \rangle$ vanishes if $|n\rangle$ belongs to another symmetry subspace. In this paper, the excitation energy $E_n - E_0$ of the lowest eigenstate with a non-zero matrix element $\langle 0 | \hat{J} | n \rangle$ is called the optical gap E_{opt}.

III. NUMERICAL METHODS

DMRG[19,20] is known to be a very accurate method for one-dimensional quantum systems with short-range interactions such as the extended Hubbard Hamiltonian (1). In this work I use three different DMRG techniques to calculate ground states, excited states, and dynamic response functions. All three techniques are based on the finite system DMRG algorithm.

First, the usual ground-state DMRG method is used to calculate the ground state $|0\rangle$ for a fixed number N_σ of electrons of each spin σ. This method provides the ground-state energy $E_0(N_\uparrow, N_\downarrow)$ and allows us to calculate ground-state expectation values $\langle 0 | \hat{O} | 0 \rangle$ for various operators $\hat{O}$, such as static correlation functions. The (Mott) gap E_M in the single-particle density of states of a Mott insulator can also be obtained using this approach. At half filling ($N_\sigma = N/2$) the Mott gap is simply given by

$$
E_M = 2 \left[\; E_0(N_\uparrow + 1, N_\downarrow) - \; E_0(N_\uparrow, N_\downarrow) \; \right]
\tag{5}
$$

because of the charge-conjugation symmetry.

Second, a symmetrized DMRG[29] technique is used to calculate the lowest eigenstates $|n\rangle$ in the B_u^- symmetry sector. This method yields not only the eigenenergies E_n of the lowest optically excited states (in particular, the optical gap E_{opt}), but also allow us to compute expectation values $\langle n | \hat{O} | n \rangle$ and thus to analyze the nature of these states. To optimize the DMRG program performance, my implementation of the charge-conjugation

and spin-flip symmetries differs from the original idea presented in Ref. 29. This is explained in detail in appendix.

Finally, the dynamical DMRG method[11,21] is used to compute the optical conductivity (2) convolved with a Lorentzian distribution of width $\eta > 0$. Comparisons with exact results have shown that DDMRG is a very reliable numerical method, which yields spectra with an accuracy comparable to exact diagonalizations but for much larger systems.[11,13,21]

All DMRG methods have a truncation error which is reduced by increasing the number m of density-matrix eigenstates kept (for more details, see Refs. 19 and 20). Varying m allows one to compute physical quantities (including spectra) for different truncation errors and thus to obtain error estimates on these quantities. I have systematically used this procedure to estimate the precision of my numerical calculations and adjusted the maximal number m of density-matrix states to reach a desired accuracy. The largest number of density-matrix eigenstates used in this work is $m = 1000$. For all numerical results presented in this paper DMRG truncation errors are negligible.

All numerical calculations have been performed on lattices with an even number N of sites using open boundary conditions. As we are interested in the properties of the Hamiltonian (1) in the thermodynamic limit, numerical calculations have always been carried out for several system sizes N in order to investigate finite-size effects. The largest system size used here is $N = 512$. If necessary, the results have been extrapolated to the infinite system limit $N \to \infty$. To evaluate finite-size effects in a continuous spectrum one has to compute it for different sizes while keeping $\eta N = \text{const.}$[21] In this work $\eta N = 12.8t$ is used. For all numerical results presented in this paper finite-size effects (including chain-end effects) are negligible unless discussed explicitly. For spectra this means that finite-size effects are completely hidden by the broadening η. More precisely, DDMRG results for finite $N = 12.8t/\eta$ are not distinguishable from the corresponding infinite-system spectra convolved with a Lorentzian distribution of width η (see the discussion in Ref. 21).

IV. RESULTS

To facilitate the comparison with analytical results, the discussion of optical excitations in the Mott insulating phase is divided in three subsections: the limit of a large Mott gap, the regime of finite Mott gaps, and the limit of a small Mott gap. Note, however, that the Mott gap E_M just fixes the energy scale; the minimal energy required to create a charge excitation is $E_M/2$ but optical excitations do not differ qualitatively as E_M varies if everything else is kept constant. In all cases, there is spin-charge separation and the spin sector is gapless. Elementary excitations in the charge sector are spinless bosons in the lower and upper Hubbard bands. Optical excitations are always made of an even number (≥ 2) of elementary excitations with opposite charges (to preserve charge neutrality). The different types of optical excitations and optical spectra found in the model (1) result from the residual interactions (essentially the non-local part of the Coulomb repulsion, here V) between the elementary charge excitations.

A. Limit of a large Mott gap

In the strong-coupling limit $U \gg t$, the properties of the model (1) in the Mott insulating phase can be described using simple concepts. In the ground state double occupation is prohibited and there is exactly one electron on each site. Elementary charge excitations can be represented as an empty site (holon in the lower Hubbard band) or a doubly occupied site (doublon in the upper Hubbard band). The minimal energy required to create a holon or a doublon is $E_M/2 = U/2 - O(t) \gg t$. Optical excitations always consist of an equal number of holons and doublons to conserve the total charge. The ionicity of excited states is defined as the change in the number of doubly occupied sites with respect to the ground state

$$I_n = \langle n|\hat{N}_d|n\rangle - \langle 0|\hat{N}_d|0\rangle \;, \tag{6}$$

where $\hat{N}_d = \sum_l \hat{n}_{l,\uparrow}\hat{n}_{l,\downarrow}$ and $|0\rangle, |n\rangle$ denote the ground state and excited states, respectively. Thus, I_n is a measure of the number of doublons (or equivalently of holons) created by an excitation. Depending on the strength of the nearest-neighbor interaction parameter V, the low-energy optical excitations are made of a single doublon-holon pair ($I_n = 1$) or are collective excitations of several such pairs ($I_n > 1$). Note that I_n is also equal to the derivative of the excitation energy $E_n - E_0$ with respect to U.

Single holon-doublon pair

For $V < U/3 + O(t)$, optical excitations consist of a single holon-doublon pair and the optical properties, which can be calculated exactly,[14,15] depend only on the parameters V and t. For $0 \leq V \leq 2t$, holon and doublon are independent. A schematic representation of this state is shown in Fig. 1. This pair of free charge excitations gives rise to a continuous band in the optical spectrum $\sigma_1(\omega)$. The band starts at the Mott gap $E_M = U - 4t$ and has a width of $8t$. As there is no optical excitation with a lower energy than E_M, the Mott gap is also the optical gap E_{opt}. The optical spectra for $V = 0$ and $V = 2t$ are shown in Fig. 2 with a broadening $\eta/t = 0.1$. At the conductivity threshold $\sigma_1(\omega)$ vanishes as $\sqrt{\omega - E_M}$ for $V < 2t$ but diverges as $1/\sqrt{\omega - E_M}$ in the special case $V = 2t$. The optical conductivity also has a small peak at $\omega = U - V$ with 1 % of the spectral weight.[13] This peak is visible inside the band for $V = 0$ and $V = 2t$ in Fig. 2.
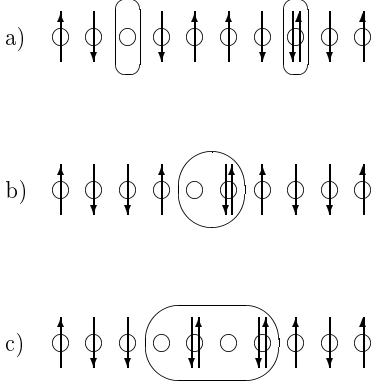
FIG. 1: Schematic representation of (a) an unbound holon-doublon pair, (b) an exciton, and (c) a biexciton in the strong-coupling limit $U - 2V \gg t$.
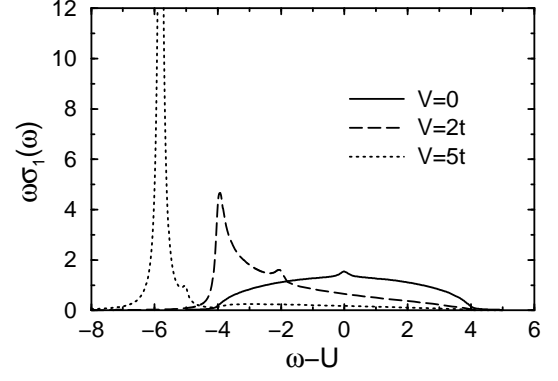

FIG. 2: Reduced optical conductivity $\omega\sigma_1(\omega)$ in the limit of a large Mott gap ($U \gg t$) calculated with DDMRG for three different values of V using $\eta/t = 0.1$ ($N = 128$ sites).

It corresponds to a bound state made of dispersionless charge excitations[14] and can be seen as a localized exciton with size $\xi = 1$.

For $V > 2t$, there is also a continuous band starting at $\omega = E_M = U - 4t$ due to independent holon-doublon pairs, but the lowest optical excitation is now an exciton (i.e., a bound holon-doublon pair) with an energy $\omega_{\text{exc}} = E_{\text{opt}} = U - V - 4t^2/V$ (Ref. 14). The term $-4t^2/V$ is the kinetic energy lowering due to the exciton center-of-mass motion. Therefore, in the strong-coupling limit ($U \gg t$) the exciton binding energy is $E_b = E_M - E_{\text{opt}} = V - 4t + 4t^2/V$ ($V > 2t$). This binding energy significantly differs from the incorrect result $E_b = V$ often reported in the literature,[26] which is (approximately) valid only under the additional condition $V \gg t$. In the optical spectrum $\sigma_1(\omega)$ the exciton generates an isolated δ-peak at ω_{exc} below the band onset. For $V \gg t$, an exciton is essentially the nearest-neighbor holon-doublon pair shown in Fig. 1. This is exactly the state generated by the current operator (4) applied to the ground state with one electron on each site. Thus the spectral weight is concentrated in the excitonic peak for $V \gg t$. This strong excitonic peak is already clearly visible for $V = 5t$ in Fig. 2. For finite V/t, however, there is a finite probability of finding holon and doublon at a distance $m > 1$. This probability can be calculated exactly[13]

$$C(m) = C(1 - \delta_{m,0})e^{-\kappa m} \qquad (7)$$

with $\kappa = 2\ln(V/2t)$ and a normalization constant C. The exciton size (the average holon-doublon distance) is then

$$\xi(V > 2t) = \frac{V^2}{V^2 - 4t^2} \qquad (8)$$

and decreases as V increases. Correspondingly, one observes a progressive transfer of spectral weight from the band above E_M to the excitonic peak at $\omega_{\text{exc}} = U - V - 4t^2/V$ as V increases. Note that, as for $V \leq 2t$,

there is a small peak corresponding to a localized exciton at $\omega = U - V$ in the optical conductivity. This peak lies in the band for $V < 4t$ but is situated between the band and the strong excitonic peak for $V > 4t$. In Fig. 2 it can be seen for $V = 5t$ as a small bump at the foot of the strong peak.

Figure 2 shows optical spectra calculated with the DDMRG method on a 128-site lattice. On the scale of this figure, the DDMRG spectra are indistinguishable from the analytical results for an infinite system.[13,14] (For an expanded view showing small deviations, see Fig. 1 of Ref. 13.) This perfect agreement confirms the validity of the strong-coupling calculations done in Ref. 14. Moreover, it confirms once more that DDMRG can accurately reproduce infinite-system optical spectra.[21]

Collective excitations

As we have just seen, the creation energy of an excited state with ionicity $I_n = 1$ is either $U - O(t)$ for an unbound holon-doublon pair or $U - V - O(t^2/V)$ for an exciton. Once a first excitation has been created, however, the creation of a second holon-doublon pair bound to the first excitation requires only an energy $U - 2V$. Therefore, when V becomes large enough, the lowest optical excitations are bound states of n_{exc} excitons, called excitonic strings.[31,32] A biexciton ($n_{\text{exc}} = 2$) is shown in Fig. 1 as an illustration (see also Ref. 9).

The excitation energy of a n_{exc}-exciton string is

$$E(n_{\text{exc}}) = U - V + (n_{\text{exc}} - 1)(U - 2V) - O(t^2/V) . \quad (9)$$

Here the correction of order t^2/V corresponds to the kinetic energy lowering due to the center-of-mass motion. An n_{exc}-exciton string ($n_{\text{exc}} \geq 2$) appears in the low-energy excitation spectrum, around or below the onset $E_M = U - 4t$ of the band of free holons and doublons, if $E(n_{\text{exc}}) \lesssim E_M$ or

$$V \gtrsim \frac{n_{\text{exc}} - 1}{2n_{\text{exc}} - 1}U + O(t) . \qquad (10)$$

Thus, the biexciton becomes a low-energy excitation for $V \gtrsim U/3$ and longer excitonic strings ($n_{\text{exc}} \geq 3$) for larger V. The case $n_{\text{exc}} = 1$ corresponds to the usual exciton, which appears in the low-energy spectrum as soon as $V > 2t$ as discussed above. As an n_{exc}-exciton string is made of n_{exc} doublons and holons bound together, it is a neutral excitation, its ionicity is $I = n_{\text{exc}}$, and its length is $2n_{\text{exc}} - 1$ in units of the lattice constant. Excitonic strings have been observed in the *non-linear* optical spectrum of quasi-one-dimensional neutral mixed-stack charge-transfer solids and are known to contribute to the *non-linear* optical conductivity of models such as the extended Hubbard model (1).[9,31] Naively, one does not expect excitonic strings with $I = n_{\text{exc}} \geq 2$ to contribute to the *linear* optical spectrum $\sigma_1(\omega)$. In the limit $U/t \gg t$ the current operator (4) creates at most one holon-doublon pair and thus in Eq. (3) the matrix elements $\langle n|\hat{J}|0\rangle$ between an excited state $|n\rangle$ and the ground state $|0\rangle$ must vanish if the ionicity (6) is larger than 1. Yet, we will see in the next section that excitonic strings with $n_{exc} \geq 2$ are visible in the *linear* optical conductivity of the extended Hubbard model for large but finite couplings U/t and V/t. The reason is that for any finite t there are quantum charge fluctuations (virtual holon-doublon pairs) in all eigenstates of the Hamiltonian (1) which leads to small but finite matrix elements $\langle n|\hat{J}|0\rangle$ even if the average ionicity I_n of an excitation $|n\rangle$ exceeds one,

$$\langle n|\hat{J}|0\rangle \sim \left(\frac{t}{U - 2V}\right)^{(I_n - 1)} . \qquad (11)$$

Thus, for $V \gtrsim U/3 \gg t$ the low-energy optical spectrum consists of a strong excitonic peak at $\omega = E_{\text{opt}} = U - V - O(t^2/V)$ followed by several [$n_{\text{exc}} = 2, 3, \ldots \lesssim (U - V)/(U - 2V)$] weaker isolated δ-peaks with exponentially decreasing spectral weight at $\omega \approx E_{\text{opt}} + (n_{\text{exc}} - 1)(U - 2V)$. All these peaks appears below (or about) the onset of a weak continuum due to free holons and doublons at $\omega = E_M$.

As long as $U - 2V \gg t$, excitonic strings retain a well-defined size represented by an integer number n_{exc} because the kinetic energy lowering $\sim t$ due to size fluctuations is much smaller than the energy cost $\sim (U - 2V)$ per exciton in the string. Close to the phase boundary ($U \approx 2V$) between the CDW ground state and the Mott insulator,[22,23] however, size fluctuations become advantageous. Thus, for $U - 2V \lesssim t$ low-energy excitations (of the Mott insulator) are CDW droplets, which can be understood as superpositions of excitonic strings of every size,

$$|\psi\rangle = c_1|n_{\text{exc}} = 1\rangle + c_2|n_{\text{exc}} = 2\rangle + c_3|n_{\text{exc}} = 3\rangle + \ldots \qquad (12)$$

with a broad distribution of coefficients c_n ($\sum_n |c_n|^2 = 1$). For $U - 2V \to 0^+$ the distribution becomes flat, i.e., $|c_n|^2 \to$ const. (For comparison, an n_{exc}-exciton string can be described by the above state with $|c_n|^2 \approx 1$ for $n = n_{\text{exc}}$ and $|c_n|^2 \ll 1$ for $n \neq n_{\text{exc}}$.) CDW droplets in the Mott insulating phase are the analogue to the SDW droplets in the CDW insulator discussed by Hirsch.[22] As excitonic strings, these CDW droplets are neutral excitations, but one can generalize the concept to CDW droplets carrying charges (see below). The average size r_{CDW} of a CDW droplet is related to its ionicity by $r_{\text{CDW}} = 2I = 2\sum_i i|c_i|^2$. Its excitation energy is

$$E(r_{\text{CDW}}) = U - V + \frac{r_{\text{CDW}}}{2}(U - 2V) - st , \qquad (13)$$

where $s > 0$ and $-st$ represents the kinetic energy lowering due to droplet size fluctuations and center-of-mass motion ($s \approx 4$ for $U - 2V \to 0^+$). Contrary to excitonic strings, the ionicity I of a CDW droplet is not a integer number but can take any value ≥ 1. Therefore, for $U - 2V \ll t$ there is a band of CDW droplet excitations starting at $U - V - st$. Moreover, the matrix element $\langle n|\hat{J}|0\rangle$ for a CDW droplet $|n\rangle$ is essentially given by the overlap c_1 with the single exciton state in Eq. (12). Thus in this regime one expects that the CDW droplets give rise to a band in the optical spectrum $\sigma_1(\omega)$ starting at $\omega = E_{\text{opt}} = U - V - st$. This band lies below the Mott gap E_M. It should be noted that the Mott gap is determined by the excitation energy of unbound holons and doublons, $E_M \approx U - 4t$, as long as $U - 2V \gg t$. For $U - 2V \lesssim t$, however, CDW droplets carrying a charge $\pm e$ [a CDW droplet (12) bound to an extra holon or doublon] have a lower energy than a bare holon or doublon and reduce the gap for charge excitations (5) to $E_M = U - s't$ with $s' \approx 8$ for $V \to U/2$.

In summary, in the limit of a large Mott gap ($U \gg t$) there are four distinct regimes corresponding to four types of excitations in the low-energy optical spectrum: independent charge excitations for $V \leq 2t$, excitons for $V > 2t$ but $V \lesssim U/3$, excitonic strings for $V \gtrsim U/3 \gg t$ but $U - 2V \gtrsim t$, and CDW droplets for $U - 2V \lesssim t$. We will see that these excitations are also found in the optical spectrum of the extended Hubbard model for finite interaction strengths and Mott gaps.

B. Regime of finite Mott gaps

For finite coupling parameters U and V the low-energy optical properties of the extended Hubbard model (1) can be calculated using the ground-state and symmetrized DMRG methods presented in Sec. III. Figure 3 shows the Mott gap E_M and the optical gap E_{opt} as a function of V for three values of U. Both gaps increase monotonically with U but decrease with increasing nearest-neighbor interaction V.[26,27] For all values of U the optical gap equals the Mott gap (in the thermodynamic limit) as long as $V \leq 2t$ but for larger V, E_{opt} becomes smaller than E_M. This suggests that for all $U > 0$ the low-energy excitations are unbound for $V \leq 2t$ and bound for $V > 2t$ as in the $U \gg t$ limit.[14,26] Obviously, the condition $V > 2t$ can be realized only for relatively strong coupling ($U \gtrsim 4t$) because the Mott insulating phase exists only for V up
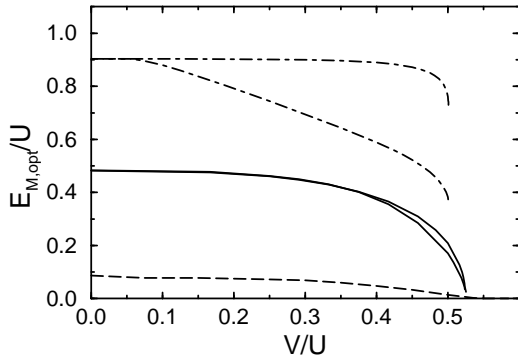
FIG. 3: Mott gap E_M (upper line) and optical gap E_{opt} (lower line) versus V for $U/t = 40$ (dot-dashed), 6 (solid), and 2 (dashed). For $U = 2t$, $E_{\mathrm{opt}} = E_M$.

to $V_c \approx U/2$. The Mott gaps in Fig. 3 are initially almost constant as V increases then diminish significantly close to the phase boundary V_c. This agrees with the strong-coupling analysis in the previous section, which suggests that E_M is essentially independent of V for $V_c - V \gg t$ but is reduced by quantity $\propto t$ as V approaches the critical value V_c. Note that on the critical line between the CDW and Mott insulating phases, both gaps vanish for $U \leq 3t$ while the Mott gap clearly remains finite for stronger coupling ($U \geq 4t$).

To determine the nature of the low-energy optical excitations I have calculated their ionicity (6). Figure 4 shows the ionicity I_1 of the first optically excited state (the $1B_u^-$ state) as a function of V for three values of U. In the half-filled Hubbard model ($V = 0$) I_1 increases monotonically from 0 at $U = 0$ to 1 for $U \to \infty$, reflecting the increasingly ionic nature of the elementary charge excitations in the lower and upper Hubbard bands. The ionicity increases slowly with V and remains below or close to 1 for most couplings (U, V), which confirms that the corresponding optical excitations are made of a single pair of elementary charge excitations. In the regime $U \approx 2V > 4t$, however, one observes a rapid but continuous increase of I_1 to values larger than 2 as $V \to V_c \approx U/2$. This shows that the lowest optical excitation has become a CDW droplet. Looking at higher optical excitations, one finds the same qualitative behavior of the ionicity as a function of U and V. Additionally, one observes the formation of excitonic string with integer $I = n_{\mathrm{exc}} \geq 2$.

To determine whether the pair of elementary charge excitations form bound (exciton) or unbound states, one can calculate the average distance between both excitations using an exciton correlation function.[13,33,34] For $V < 2t$ I have found that this average distance always diverges with increasing system size N. This result definitively confirms that in this regime an optical excitation is a pair of independent charge excitations, in agreement with the strong-coupling analysis. For $V > 2t$, the average distance tends to a finite value for $N \to \infty$ as
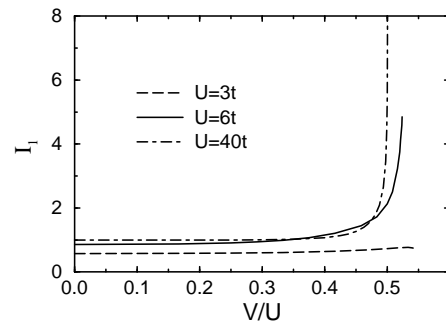

FIG. 4: Ionicity I_1 of the first optically excited state ($1B_u^-$) as a function of V for three different values of U.

expected for an exciton. The exciton size ξ determined with this procedure is shown in Fig. 5 as a function of V for two finite values of U. The exciton size in the limit $U \gg t$, Eq. (8), is also plotted for comparison. The size ξ increases and diverges as V tends to $2t$, showing the unbinding of the exciton at $V = 2t$. Note that for $U = 40t$ the sizes measured with the exciton correlation function[13,33,34] agree perfectly with Eq. (8).

One can gain some knowledge about the nature of optically excited states by looking at the scaling of their spectral weight

$$W_n = \frac{\pi}{Na} \frac{|\langle n|\hat{J}|0\rangle|^2}{E_n - E_0} \tag{14}$$

[see Eqs. (2) and (3)] with the system size N. For $V \leq 2t$ I have found that the spectral weight of low-lying excitations vanishes for $N \to \infty$, which is expected for states belonging to a continuum. (As there is an infinite number of states in a continuous band, the spectral weight of each state must go to zero as $N \to \infty$, so that the total weight in any finite frequency interval remains finite.) For $V > 2t$ (but outside the CDW droplet regime), I have found that the optical weight W_1 of the $1B_u^-$ state tends to a finite value in the thermodynamic limit. This corresponds to a δ-peak (with total weight $\geq W_1$) in the
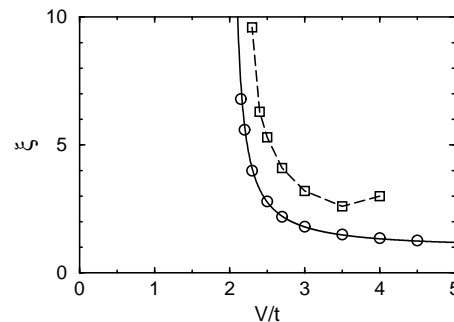

FIG. 5: Exciton size as a function of V for $U = 40t$ (circles) and $U = 8t$ (squares). The solid line is the $U \gg t$ result, Eq. (8). The dashed line is just a guide for the eyes.
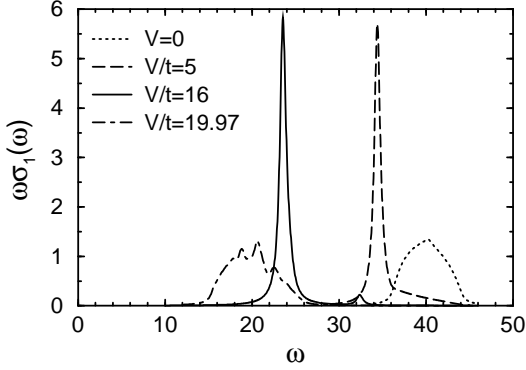
FIG. 6: Reduced optical conductivity $\omega\sigma_1(\omega)$ for $U = 40t$ and four different values of V calculated using DDMRG with $\eta/t = 0.4$ ($N = 32$ sites).
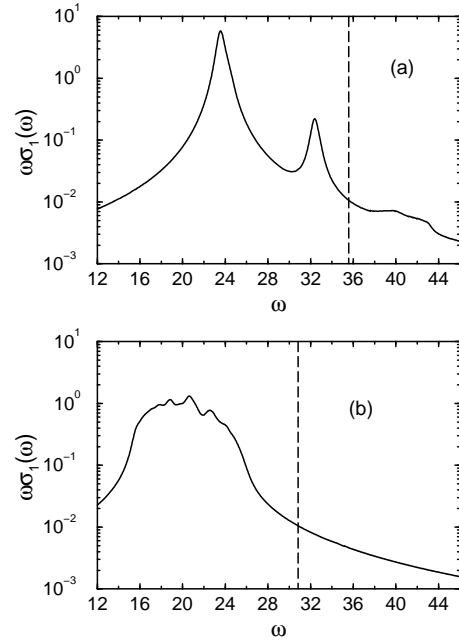

FIG. 7: Reduced optical conductivity $\omega\sigma_1(\omega)$ for $U = 40t$ and (a) $V = 16t$ and (b) $V = 19.97t$ calculated using DDMRG with $\eta/t = 0.4$ ($N = 32$ sites). Vertical lines indicate the Mott gap E_M.

optical spectrum as expected for an exciton or an excitonic string. In the CDW droplet regime, finite-size effects become large and complex and, in most cases, it has not been possible to determine the scaling of the spectral weights (14).

Optical spectra

The above analysis shows that low-energy optical excitations in the regime of finite Mott gaps are identical to those found in the limit of a large Mott gap and can be interpreted using the simple theory developed for the strong-coupling limit in Sec. IV A. Turning next to the optical spectrum I have calculated $\sigma_1(\omega)$ for various parameters $40t \geq U \geq 3t$ and $U/2 \gtrsim V \geq 0$ using the DDMRG method. I have found that the optical spectra of systems with a finite Mott gap closely resemble those observed in the limit of a large Mott gap.

As a first example, the optical conductivity $\sigma_1(\omega)$ is shown in Fig. 6 for $U = 40t$ and several values of V representing the four different regimes: free charge excitations ($V = 0$), excitons ($V = 5t$), excitonic strings ($V = 16t$), and CDW droplets ($V = 19.97t$). For $V = 0$ there is a single continuous band starting at $\omega = E_{opt} = E_M = 36.14t$. At the band edges the optical conductivity vanishes as $\sqrt{\omega - E_M}$ as discussed in Ref. 11.

For $V = 5t$ a strong excitonic δ-peak appears at $\omega_{exc} = E_{opt} = 34.39t$ below the Mott gap $E_M = 36.13t$. The exciton has a size $\xi \approx 1.2$ in perfect agreement with Eq. (8). There is also a weak continuous band of free charge excitations above E_M, which is only visible as a high-frequency tail of the exciton peak in Fig. 6. The gap between the excitonic peak and the band is not visible in Fig. 6 because of the large broadening $\eta/t = 0.4$ used here, but it can be checked with a scaling analysis for $\eta \to 0$ ($N \to \infty$) as discussed in Ref. 21. The only qualitative difference between the present result for $U = 40t$ and the corresponding result in the limit $U \gg t$

(see Fig. 1 in Ref. 13) is the absence of the weak peak associated with a localized exciton at $\omega = U - V$. Nevertheless, this weak peak is not an artifact of the strong-coupling limit because its existence has been confirmed in the Hubbard model ($V = 0$) down to $U = 4t$ (Ref. 11). The finite spectral weight carried by the localized exciton originates from a ground-state dimer-dimer correlation of the spin degrees of freedom.[14] In the strong-coupling limit ($U - 2V \gg t$) of the extended Hubbard model (1), the effective exchange coupling between nearest-neighbor spins depends on the occupation of the neighboring sites if $V \neq 0$. Thus the effective spin Hamiltonian is not the one-dimensional Heisenberg model, in general. Only for $V = 0$ or in the limit $U \gg V$, the effective spin Hamiltonian reduces to the Heisenberg model with a constant exchange coupling $J = 4t^2/U$. In this case, the ground state has the relevant spin dimer-dimer correlations and the localized exciton carried a finite optical weight as explained in detail in Ref. 14. For finite U and V, however, the spin dimer-dimer correlation is presumably destroyed by the fluctuations of the spin exchange coupling and thus the optical weight of the localized exciton vanishes.

For $V = 16t$ the condition $V \gtrsim U/3$ is satisfied and excitonic strings appear in the optical spectrum below or around the Mott gap $E_M = 35.58t$. As seen in Fig. 6, most of the spectral weight is concentrated in the exciton of size $\xi = 1.0$ at $\omega_{exc} = E_{opt} = 23.53t \approx U - V$. The biexciton at $\omega = 32.35t \approx 2U - 3V$ is barely visible in Fig. 6. The optical conductivity $\sigma_1(\omega)$ is again shown in Fig. 7(a) on a logarithmic scale. The isolated peaks
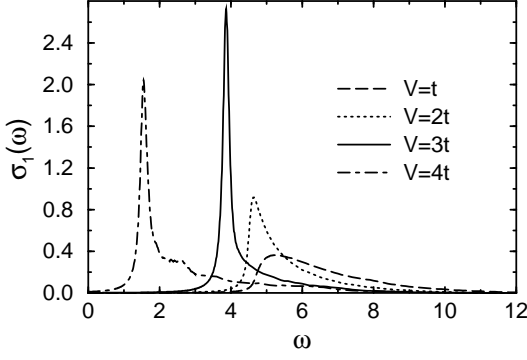
FIG. 8: Optical conductivity $\sigma_1(\omega)$ for $U = 8t$ and four different values of V calculated with DDMRG using $\eta/t = 0.1$ ($N = 128$ sites).

associated with both excitations are now clearly visible. The measured ionicity (6) is $I = 1.1$ and $I = 2.2$ for the exciton and the biexciton, respectively. In Fig. 7(a) the remnant of the continuous band of free charge excitations and the triexciton (at $\omega \approx 3U - 5V = 40t$) are also visible in the interval $\omega = 36 - 44t$ above the Mott gap.

For $V = 19.97t \approx U/2$ the optical conductivity spectrum is radically different. The excitonic strings collapse into a band of CDW droplets with varying sizes. For instance, the $1B_u^-$ state is a droplet of size $r_{CDW} = 8.9$ with an energy $E_{opt} \approx 15.5t$. These CDW droplets give rise to a broad band in the optical conductivity spectrum shown in Fig. 6. The onset of this band is well below the Mott gap $E_M = 30.83t$. On the logarithmic scale of Fig. 7(b), one sees that, in this particular case, the entire optical weight seems to be below E_M (for $\eta \to 0$). The appearance of a band below the Mott gap is also visible in the current-current correlations for $U = 12t$ and $V = 6t$ presented in Ref. 27 but the optical spectrum in the regime $U \approx 2V$ is not interpreted correctly in that work.

As a second example and to illustrate the finite-size-scaling analysis I have carried out for dynamical spectra, I discuss the optical conductivity $\sigma_1(\omega)$ for $U = 8t$. Figure 8 shows the evolution of the optical conductivity for increasing nearest-neighbor repulsion V. For $V = t$ and $V = 2t$, the spectrum contains a single continuous band due to free charge excitations starting at $E_{opt} = E_M = 4.67t$ and $4.53t$, respectively. For $V = 3t$ the spectrum consists of a strong peak corresponding to an exciton of size $\xi = 3.2$ and energy $\omega_{exc} = E_{opt} = 3.86t$, and of a weak band above the Mott gap $E_M = 4.10t$. This band is visible in Fig. 8 as the high-frequency tail of the excitonic peak. For $V = 4t$, CDW droplets of varying sizes dominate the optical spectrum. For instance, the $1B_u^-$ state is a droplet of size $r_{CDW} = 5.6$ with an excitation energy $E_{opt} = 1.55t$ lower than the Mott gap $E_M = 2.29t$. There is no intermediate regime with well-defined excitonic strings for this value of U.

The precise shape of $\sigma_1(\omega)$ cannot be determined from the sole results shown in Fig. 8 because of the finite res-
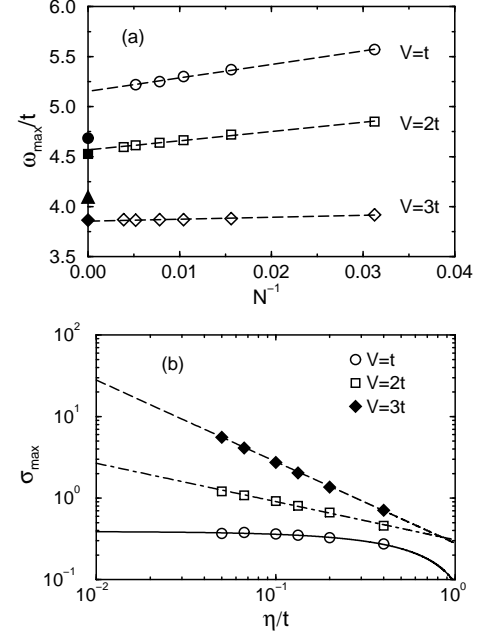

FIG. 9: Scaling analysis of the maximum in DDMRG optical spectra $\sigma_1(\omega)$ for $U = 8t$ and three different values of V ($\eta N = 12.8t$). (a) Position ω_{max} of the maximum (open symbols) as a function of the inverse system size. Lines are linear fits to these data. Solid symbols show the optical gaps E_{opt} calculated with symmetrized DMRG for $N \to \infty$. For $V = 3t$, the Mott gap E_M is indicated by a triangle. For $V/t = 1$ and 2, $E_M = E_{opt}$. (b) Maximum of $\sigma_1(\omega)$ as a function of η/t. Lines are fits to the numerical data: the dashed line corresponds to η^{-1}, the dot-dashed to $\eta^{-1/2}$, and the solid line is a linear fit in η.

olution and system size used, $\eta/t = 12.8/N = 0.1$. To determine the properties of $\sigma_1(\omega)$ with maximal resolution ($\eta \to 0$) in the thermodynamic limit ($N \to \infty$), one can perform a scaling analysis with $\eta N = const.$ as explained in Ref. 21. (Here I have used $\eta N = 12.8t$.) The scaling analysis of the optical conductivity $\sigma_1(\omega)$ calculated with DDMRG always yields results which are qualitatively and quantitatively consistent with the properties of low-lying optical excitations determined using the ground-state and symmetrized DMRG methods. For instance, $\sigma_1(\omega)$ vanishes for all $\omega < E_{opt}$ and there is a continuous band for $\omega \geq E_{opt}$ or a δ-peak at $\omega = E_{opt}$ in the limit $\eta \sim 1/N \to 0$.

The scaling analysis of the conductivity maximum $\sigma_{max} = \sigma_1(\omega_{max})$ in DDMRG spectra is illustrated in Fig. 9 for the same interaction parameters as in Fig. 8. For $V = t$, ω_{max} tends to a value ($5.15t$) larger than the optical gap $E_{opt} = 4.67t$ calculated with symmetrized DMRG for $N \to \infty$ [see Fig. 9(a)] while σ_{max} tends to a finite value for $\eta \to 0$ [see Fig. 9(b)]. Moreover, the derivative of $\sigma_1(\omega)$ has a maximum that diverges as $1/\sqrt{\eta}$ for $\eta \to 0$ at $\omega = E_{opt}$. These features correspond to a continuum that vanishes as $\sqrt{\omega - E_{opt}}$ at the conductivity threshold and goes through a maximum just above

the optical gap at $\omega_{\max} \approx 1.1 E_{\text{opt}}$ (see Ref. 21). For $V = 2t$, $\omega_{\max}$ tends to the same value as the optical gap E_{opt} for $N \to \infty$ [see Fig. 9(a)] and $\sigma_{\max}$ diverges as $1/\sqrt{\eta}$ for $\eta \to 0$ [see Fig. 9(b)]. These features correspond to a continuum that diverges as $1/\sqrt{\omega - E_{\text{opt}}}$ at the conductivity threshold.[21] (Note that for all values of U investigated $\sigma_1(\omega)$ displays this divergence at $V = 2t$.) Therefore, the features of the optical spectrum for $V \leq 2t$ are similar to those found in the strong-coupling limit. For $V = 3t$, $\omega_{\max}$ tends for $N \to \infty$ to the same value as the optical gap E_{opt} (which is smaller than the Mott gap in the thermodynamic limit) [see Fig. 9(a)] and $\sigma_{\max}$ diverges as $1/\eta$ for $\eta \to 0$ [see Fig. 9(b)]. These features correspond to a δ-peak at $\omega = E_{\text{opt}}$. Moreover, $\sigma_1(\omega)$ vanishes between E_{opt} and E_M but remains finite above E_M in the limit $\eta \sim 1/N \to 0$. Therefore, in the thermodynamic limit the spectrum for $V = 3t$ (shown in Fig. 8 for $N = 128$ sites) consists of an excitonic δ-peak separated from the band of independent charge excitations as in the strong-coupling limit. In the CDW droplet regime (i.e., close to the critical line $V_c \approx U/2$ separating Mott and CDW phases) finite-size effects are more complicated and larger than in the other regimes. As a consequence, for $V = 4t$ it has not been possible to perform a conclusive analysis with the largest system sizes ($N = 256$) available. It seems that the low-energy spectrum contains a δ-peak at E_{opt} and a band starting immediately above E_{opt}, both due to CDW droplets.

In summary, I have found that the optical properties for all finite Mott gaps (i.e., for all $U > 0$, $V \geq 0$ in the Mott phase) are qualitatively similar to those calculated in the limit of a large Mott gap (Sec. IV A, Refs. 13, 14):

(i) For $V \leq 2t$ (that is the only possible case for $U \lesssim 4t$), independent charge excitations give rise to a continuous band starting at the Mott gap E_M, which is equal to the optical gap. The band width is typically $\sim 8t$. For $V < 2t$, $\sigma_1(\omega)$ vanishes smoothly at the threshold E_{opt}, typically as $\sqrt{\omega - E_{\text{opt}}}$. At $V = 2t$, $\sigma_1(\omega)$ diverges as $1/\sqrt{\omega - E_{\text{opt}}}$ for $\omega - E_{\text{opt}} \to 0^+$.

(ii) For $V > 2t$ but $U > 2V + O(t)$ and $V < U/3 + O(t)$ (this is possible only for $U \gtrsim 4t$), the optical spectrum consists of an excitonic δ-peak below the Mott gap and a band due to free charge excitations above E_M. Most of the optical weight is in the excitonic peak for $V \gtrsim 3t$.

(iii) If U is large enough ($U \gtrsim 12t$) excitonic strings appear in the low-energy spectrum for $V > U/3 + O(t)$ but $U > 2V + O(t)$. They generate isolated δ-peaks below the Mott gap E_M in the optical conductivity $\sigma_1(\omega)$ with a separation between peaks of $\Delta\omega \approx U - 2V$. The first peak is an exciton and contains most of the spectral weight. A very weak band due to free charge excitations still exists above E_M.

(iv) Close to the boundary $V_c \approx U/2$ between the Mott and CDW phases, if V exceeds $2t$, CDW droplets dominate the low-energy spectrum and give rise to a broad band (including sharp peaks) starting below the gap for charge excitations (5).

TABLE I: Mott gap E_M, optical gap E_{opt}, ionicity I_1 of the first optically excited state $1B_u^-$, and the corresponding field-theory interaction parameter β^2 (see text) for several values of U and V in the small gap regime $E_M/t = 0.6 - 0.7$.

U/t	V/t	E_M/t	E_{opt}/t	I_1	β^2
3	0	0.631	0.628	0.574	1
3.5	1.4	0.664	0.662	0.784	0.61
4	1.9	0.628	0.627	1.11	0.52
4.15	2	0.645	0.642	1.20	1/2
4.5	2.25	0.638	0.611	1.54	(0.449)
5	2.57	0.605	0.524	2.22	(0.400)
6	3.115	0.643	0.445	4.00	(0.327)
8	4.137	0.641	0.24	19.9	-

C. Limit of a small Mott gap

In the limit of a small Mott gap ($E_M \ll t$) the coherence length $\sim 4t/E_M$ becomes very large and it is not possible to carry out numerical simulations on lattices large enough ($N \gg 4t/E_M$) to determine the optical spectrum with confidence. Fortunately, in this limit field-theoretical methods provide generic results for the low-energy optical spectrum of a one-dimensional Mott insulator.[11,12,13] Field-theoretical results are applicable to lattice models such as Eq. (1) for gaps up to $E_M \lesssim t$, which makes possible a direct quantitative comparison of field theory and DDMRG calculations.[11,13,21]

In the field-theoretical approach, elementary charge excitations are holons (in the lower Hubbard band) and anti-holons (in the upper Hubbard band). Optical excitations are made of a equal number of holons and anti-holons. Assuming that the low-energy excitations consist of one holon-antiholon pair, the optical conductivity is

$$\sigma_1^{\text{FT}}(\omega) = A \, S_\beta(\omega/E_M) \qquad (15)$$

where $S_\beta(x)$ is a known function depending on the field-theory interaction parameter $0 < \beta \leq 1$, and A is a unknown constant which sets the conductivity scale. Strictly speaking, this result is exact only for $\omega < 2E_M$ and $\beta^2 > 1/3$ but it has been found by comparison with DMRG results that corrections for $\omega > 2E_M$ are usually negligible.[11,13] For $\beta^2 \geq 1/2$, $\sigma_1^{\text{FT}}(\omega)$ describes a single continuous band starting at $E_{\text{opt}} = E_M$, which is due to independent holons and anti-holons. The optical conductivity vanishes smoothly as $\sqrt{\omega - E_{\text{opt}}}$ for $\beta^2 > 1/2$ and diverges as $1/\sqrt{\omega - E_{\text{opt}}}$ for $\beta^2 = 1/2$ at the conductivity threshold. For $1/3 < \beta^2 < 1/2$, there is a δ-peak at $\omega = E_{\text{opt}} < E_M$ in addition of the band starting at $\omega = E_M$. The δ-peak is due to a bound holon-antiholon pair (exciton). For $\beta^2 < 1/3$ additional excitons and excitonic strings (made of several holon-antiholon pairs) appear in the spectrum. Therefore, field-theoretical predictions for the optical conductivity of a one-dimensional Mott insulator are qualitatively similar to what we have
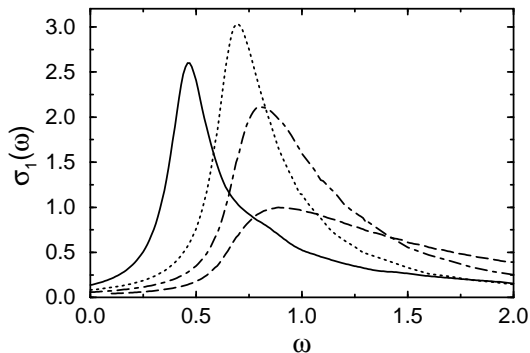
FIG. 10: Optical conductivity $\sigma_1(\omega)$ calculated with DDMRG using $\eta/t = 0.1$ ($N = 128$ sites) for $U = 3t, V = 0$ (dashed), $U = 3.5t, V = 1.4t$ (dot-dashed), $U = 4.15t, V = 2t$ (dotted), and $U = 6t, V = 3.155t$ (solid).
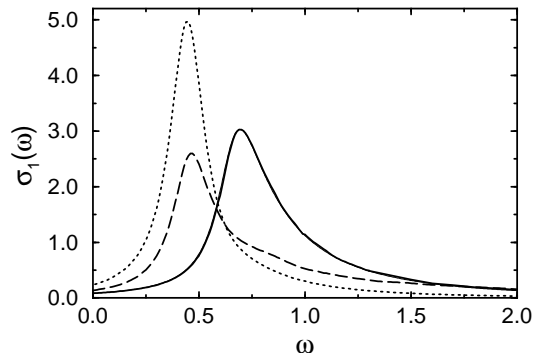

FIG. 11: Comparison of optical spectra calculated with DDMRG ($N = 128$ sites) and field theory ($N = \infty$) for $\eta/t = 0.1$. The dashed line is the DDMRG result for $U = 6t$ and $V = 3.155t$. The dotted line is the corresponding field-theoretical result ($\beta^2 = 0.327$, $E_M = 0.643t$). The DDMRG spectrum for $U = 4.15t, V = 2t$ and the field-theoretical spectrum for $\beta^2 = 1/2$, $E_M = 0.645$ are given by the solid line.

found in the extended Hubbard model (1) using a strong-coupling analysis and DDMRG simulations.

The field-theory parameters E_M, β, and A must be estimated numerically by comparison with DMRG results because one does not know their relations to the lattice model parameters U, V, t. I have first determined several couplings (U, V) which yield approximately the same Mott gap $E_M/t \approx 0.6 - 0.7$. These couplings are listed in Table I with the corresponding Mott and optical gaps calculated using the ground-state and symmetrized DMRG methods. Then I have calculated the optical conductivity $\sigma_1(\omega)$ for these parameters using DDMRG. Some results are shown in Fig. 10. Note the progressive displacement of spectral weight to lower energy as V increases although the Mott gap remains almost constant (see Table I). To determine the parameters β and A one can now compare the field-theoretical spectra with the DDMRG data. [$\sigma_1^{\text{FT}}(\omega)$ has to be convolved with a Lorentzian distribution of appropriate width η to make a direct comparison.[21]] This procedure yields the parameter β^2 listed in Table I. As expected the boundaries between independent charge excitations and excitons in the field theory and in the lattice model (1) coincide: $\beta^2 = 1/2$ corresponds to $V = 2t$.

For $V \leq 2t$ (corresponding to $\beta^2 \geq 1/2$) one can find parameters so that $\sigma_1^{\text{FT}}(\omega)$ perfectly fits the numerical data over a wide frequency range. For instance, in Fig. 11 no difference is visible between the DDMRG spectrum for $U = 4.15t$ and $V = 2t$ and the fitted field-theoretical spectrum up to $\omega = 2t \approx 3E_M$. For $V > 2t$, however, discrepancies between DDMRG and field-theory results appear and grow progressively stronger as V increases. It is no longer possible to find parameters β and A to reproduce the DDMRG spectra over a significant frequency range above $\omega = E_{\text{opt}}$. Instead β and A are set by the optical gap and the total spectral weight. This yields the values of β shown in parenthesis in Table I. As an example, one see in Fig. 11 that the field-theoretical spectrum differs significantly from the DDMRG result

for $U = 6t$ and $V = 3.115t$, although optical gap, Mott gap, and total spectral weight are identical for both spectra. The DDMRG result shows that there is substantial optical weight both at $E_{\text{opt}} = 0.445t$ and above the Mott gap $E_M = 0.643t$ while, according to field theory,[13] for a ratio $E_{\text{opt}}/E_M \approx 0.7$ the optical conductivity should be dominated by an excitonic peak at $\omega = E_{\text{opt}}$ with very little weight in the holon-antiholon band above the Mott gap E_M and in the exciton-exciton continuum above $\omega \approx 1.7E_{\text{opt}} \approx 1.1t$.

This disagreement between field theory and DDMRG results is not due to a failure of either method in the excitonic regime. It has been shown that field theory and DDMRG calculations for excitons agree very well in the extended Hubbard model with next-nearest-neighbor repulsion.[13] The problem is that the field-theory approach assumes that the low-energy optical excitations are made of two elementary charge excitations. In the extended Hubbard model (1), however, the conditions $E_M \ll 4t$ and $V > 2t$ are satisfied only close to the phase boundary $V_c = U/2$, where low-energy excitations are CDW droplets made of many elementary charge excitations. For instance, the ionicity of the $1B_u^-$ state becomes significantly larger than 1 as V increases above $2t$ as seen in Table I. Therefore, the field-theory approach is not applicable to the lattice model (1) with $V > 2t$ even in the limit of a small Mott gap. Moreover, the extended Hubbard model (1) cannot describe a Mott insulator with a small gap and an exciton in the optical spectrum for any parameters U and V.

V. CONCLUSION

I have investigated the linear (one-photon) optical excitations of a one-dimensional Mott insulator, the half-
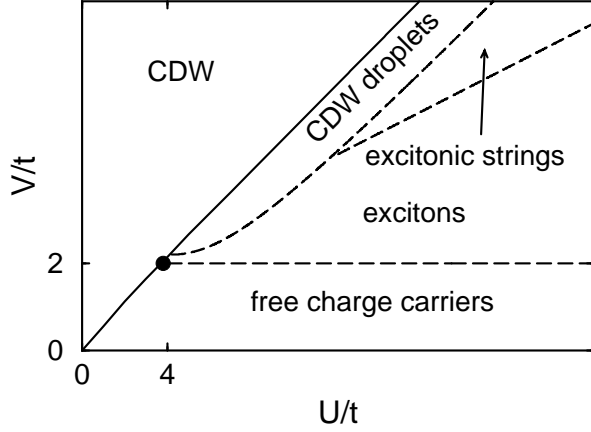
FIG. 12: Schematic representation of the different regions in the (U, V) parameter space where a particular optical excitation dominates the low-energy optical spectrum of the Mott insulating phase. The solid line is the boundary between the CDW and Mott phases.

filled extended Hubbard model, using DMRG methods. Four types of optically excited states have been found: pairs of free (unbound) charge excitation, excitons, excitonic strings, and CDW droplets. Correspondingly, there are four different regimes in the model parameter space (U, V) depending on the nature of the low-energy optical excitations. They are shown in the schematic "phase diagram" of Fig. 12. Note that only the $V = 2t$ line separating the regime of free excitations from that of bound excitations represents a sharp transition. The other dashed lines represent smooth crossover from one regime to another. In each regime one observes optical spectra with distinct features. In all cases, optical excitations are made of an even number of elementary excitations carrying opposite charges in the lower and upper Hubbard bands. The different types of excitations and optical spectra found in this system result from the residual interactions between these elementary excitations.

For $V \leq 2t$ the low-energy optical excitations are made of two unbound elementary charge excitations. They give rise to a single continuous band in the optical spectrum, starting at the Mott gap E_M, which thus equals the optical gap E_{opt}. The optical conductivity vanishes smoothly as $\sqrt{\omega - E_{\text{opt}}}$ at the threshold E_{opt}, except for $V = 2t$, where it diverges as $1/\sqrt{\omega - E_{\text{opt}}}$. For $V > 2t$ ($\Rightarrow U \gtrsim 4t$) but $V < U/3 + O(t)$ and $U - 2V \gtrsim t$, the lowest optical excitation is an exciton (a neutral excitation made of two bound elementary charge excitations) at an energy E_{opt} lower than the Mott gap E_M. This exciton gives rise to an isolated δ-peak in the optical conductivity at $\omega = E_{\text{opt}}$. Furthermore, one still finds a continuous band starting at the Mott gap E_M due to free charge excitations. For $V > U/3 + O(t)$ and $V > 2t$ but $U - 2V \gtrsim t$ ($\Rightarrow U \gtrsim 12t$) the low-energy optical excitations are excitonic strings consisting of $n_{\text{exc}} \geq 1$ excitons with energy $E(n_{\text{exc}}) \approx E_{\text{opt}} + (n_{\text{exc}} - 1)(U - 2V)$. The spectrum con-

sists of several isolated δ-peaks at $\omega = E(n_{\text{exc}}) < E_M$. In this regime one still observes a very weak band of free charge excitations starting at E_M in the spectrum. Finally, close to the CDW phase boundary ($U - 2V \lesssim t$) for $V > 2t$ the low-energy excitations are CDW droplets and give rise to a broad band starting below the Mott gap E_M.

As long as optical excitations are made of a pair of (bound or unbound) elementary charge excitations (i.e, the excitation ionicity is $I \lesssim 1$), the optical spectra calculated numerically with DDMRG agree perfectly with the analytical results obtained with a strong-coupling analysis or with field-theoretical methods. This agreement confirms the accuracy and the power of the DDMRG method for calculating dynamical spectra in the thermodynamic limit. It also confirms the wide range of validity of both analytical approaches.

Some results presented here suggest further investigations. First, in the extended Hubbard model (1) no exciton exists in the regime of a small Mott gap ($E_M \lesssim t$), which is relevant for some real materials such as conjugated polymers.[1,2] It is believed that an electron-electron interaction with a longer range[13,15,18] or a lattice dimerization[26,34] can lead to the formation of excitons in systems with small gaps. However, the precise nature of the optical excitations in such systems is still controversial.[35] The approach used here for the extended Hubbard model will enable us to determine the optical properties of these systems reliably. Second, excitonic strings appear in the *linear* optical conductivity spectrum for strong interaction $U, V \gg t$ because of the weak hybridization of excitonic strings with different sizes n_{exc}. Experimentally, excitonic strings have been observed in the *non-linear* optical absorption only.[31] It would be desirable to check if excitonic strings can be found in the linear optical absorption of materials which are believed to be large-gap one-dimensional Mott insulators such as Cu oxides and Ni halides.[5,6,17] Last, there is a clear boundary between free and bound excitations in the low-energy optical spectrum at $V = 2t$. As discussed in Ref. 23 the nature of the low-energy charge excitation seems to be correlated with the order of the transition from the Mott insulating phase to the CDW insulating phase. It is likely that the tricritical point where the transition changes from continuous to first order is located precisely on the line $V = 2t$. This suggests the existence of a hidden symmetry in the charge sector of the extended Hubbard model (1) at $V = 2t$. It would be interesting to investigate this feature further.

*

APPENDIX A

In the original implementation of the charge-conjugation and spin-flip symmetries for DMRG calculations,[29] an explicit matrix representation of the superblock Hamiltonian is built. This matrix can be projected onto a symmetry subspace with chosen parities P_c and P_s, which allows one to compute eigenstates of this symmetry and reduces the computer memory and CPU time required. In an efficient implementation of DMRG, however, an explicit representation of the superblock Hamiltonian should not be constructed (at least for quasi-one-dimensional systems with only short-range interactions). A representation in terms of tensor products of matrices uses much less memory and is also much faster.[36] Projecting this representation onto a symmetry subspace slows down the program considerably. Therefore, instead of a projection, I use an exact diagonalization technique[37] to shift the chosen symmetry subspace to lower energy.

Let $\hat{P}_c$ and $\hat{P}_s$ be the charge-conjugation and spin-flip operators for the full lattice with eigenvalues $P_c = \pm 1$ and $P_s = \pm 1$. As $\hat{P}_c$ and $\hat{P}_s$ commute with the Hamiltonian $\hat{H}$, the operator

$$\hat{H}' = \hat{H} - \lambda_c \hat{P}_c - \lambda_s \hat{P}_s \qquad (A1)$$

has the same eigenstates as $\hat{H}$ but its eigenvalues are shifted, $E'_n = E_n \pm \lambda_c \pm \lambda_s$, where the signs $\pm$ are given by the eigenstate parities P_c and P_s. It is obvious that the lowest eigenstates of $\hat{H}'$ lies in the symmetry subspace with $P_c = \lambda_c/|\lambda_c|$ and $P_s = \lambda_s/|\lambda_s|$ provided $|\lambda_c|$ and $|\lambda_s|$ are large enough. Therefore, one can simply apply the usual ground-state DMRG approach to the Hamiltonian $\hat{H}'$ with appropriate values of λ_c and λ_s to obtain the lowest eigenstates in any symmetry sector. A similar approach has already been used to shift states with high total spin S to higher energy in a DMRG calculation.[38] Using the method proposed recently for including a non-abelian symmetry group in a DMRG calculation would be a further improvement.[39]

[1] *Conjugated Conducting Polymers*, edited by H. Kiess (Springer, Berlin, 1992).

[2] *Primary Photoexcitations in Conjugated Polymers: Molecular Exciton versus Semiconductor Band Model*, edited by N.S. Sariciftci (World Scientific, Singapore, 1999).

[3] *Organic Conductors*, edited by J.-P. Farges (Marcel Dekker, New York, 1994).

[4] C. Bourbonnais and D. Jérome, in *Advances in Synthetic Metals, Twenty Years of Progress in Science and Technology*, edited by P. Bernier, S. Lefrant, and G. Bidan (Elsevier, New York, 1999), pp. 206-301.

[5] M.Z. Hasan *et al.*, Phys. Rev. Lett. **88**, 177403 (2002).

[6] H. Kishida *et al.*, Nature (London) **405**, 929 (2000).

[7] N.F. Mott, *Metal-Insulator Transitions*, 2nd ed. (Taylor & Francis, London, 1990).

[8] F. Gebhard, *The Mott Metal-Insulator Transition* (Springer, Berlin, 1997).

[9] D. Guo *et al.*, Phys. Rev. B **48**, 1433 (1993).

[10] S. Mazumdar and S.N. Dixit, Synth. Met. **28**, D463 (1989); R.M. Fye *et al.*, Phys. Rev. B **44**, 6909 (1991). J. Favand and F. Mila, Phys. Rev. B **54**, 10425 (1996).

[11] E. Jeckelmann, F. Gebhard, and F.H.L. Essler, Phys. Rev. Lett. **85**, 3910 (2000).

[12] D. Controzzi, F.H.L. Essler, and A.M. Tsvelik, Phys. Rev. Lett. **86**, 680 (2001); in *New Theoretical Approaches to Strongly Correlated Systems*, edited by A.M. Tsvelik (Kluwer, Dordrecht, 2001).

[13] F.H.L. Essler, F. Gebhard, and E. Jeckelmann, Phys. Rev. B **64**, 125119 (2001).

[14] F. Gebhard, K. Bott, M. Scheidler, P. Thomas, and S.W. Koch, Philos. Mag. B **75**, 47 (1997).

[15] F.B. Gallagher and S. Mazumdar, Phys. Rev. B **56**, 15025 (1997).

[16] W. Stephan and K. Penc, Phys. Rev. B **54**, R17269 (1996).

[17] Y. Mizuno, K. Tsutsui, T. Tohyama, and S. Maekawa, Phys. Rev. B **62** R4769 (2000).

[18] W. Barford, Phys. Rev. B **65**, 205118 (2002).

[19] S.R. White, Phys. Rev. Lett. **69**, 2863 (1992); Phys. Rev. B **48**, 10345 (1993).

[20] *Density-Matrix Renormalization*, edited by I. Peschel, X. Wang, M. Kaulke, and K. Hallberg (Springer, Berlin, 1999).

[21] E. Jeckelmann, Phys. Rev. B **66**, 045114 (2002).

[22] J.E. Hirsch, Phys. Rev. Lett. **53**, 2327 (1984).

[23] E. Jeckelmann, cond-mat/0204244 (unpublished).

[24] J. Hubbard, Proc. R. Soc. London, Ser. A **276**, 238 (1963).

[25] E.H. Lieb and F.Y. Wu, Phys. Rev. Lett. **20**, 1445 (1968).

[26] Z. Shuai, S.K. Pati, W.P. Su, J.L. Brédas, and S. Ramasesha, Phys. Rev. B **55**, 15368 (1997); Z. Shuai, J.L. Brédas, S.K. Pati, and S. Ramasesha, Phys. Rev. B **58**, 15329 (1998).

[27] S.S. Kancharla and C.J. Bolech, Phys. Rev. B **64**, 085119 (2001).

[28] N. Tomita and K. Nasu, Phys. Rev. B **63**, 085107 (2001).

[29] S. Ramasesha, S.K. Pati, H.R. Krishnamurthy, Z. Shuai, and J.L. Brédas, Phys. Rev. B. **54**, 7598 (1996).

[30] For an introduction, see H.Kuzmany, *Solid-State Spectroscopy* (Springer, Berlin, 1998).

[31] S. Mazumdar *et al.*, Chem. Phys. **104**, 9283 (1996).

[32] S. Pleutin, Phys. Rev. B **61**, 4554 (2000).

[33] J. Rissler, F. Gebhard, H. Bässler, and P. Schwerdtfeger, Phys. Rev. B **64**, 045122 (2001).

[34] J. Rissler, Ph.D. thesis, University of Marburg, 2001.

[35] M. Boman and R.J. Bursill, Phys. Rev. B **57**, 15167 (1998); R.J. Bursill *ibid.* **63**, 157101 (2001).

[36] See R.M. Noack and S.R. White, in Ref. 20.

[37] X. Zotos, in *Applications of Statistical and Field Theory Methods to Condensed Matter*, edited by D. Baeriswyl, A.R. Bishop, and J. Carmelo (Plenum Press, New York, 1990).

[38] S. Daul and R.M. Noack, Phys. Rev. B **58**, 2635 (1998).

[39] I.P. McCulloch and M. Gulácsi, Europhys. Lett. **57**, 852 (2002).